Molecular Structure of the S_2 State with a g = 5 Signal in the Oxygen Evolving Complex of Photosystem II

Shota Taguchi[†], Takumi Noguchi[†] and Hiroyuki Mino[†*]

[†]Division of Material Science, Graduate School of Science, Nagoya University, Furo-cho, Chikusa-ku, 464-8602, Nagoya, Aichi, Japan.

ABSTRACT: The *g*-factor shift of the g = 4.1 EPR signal was detected in spinach PsbO/P/Q-depleted PS II. The effective g-factor of the signal shifts up to ~4.9, depending on Ca^{2+} concentration. Hyperfine structure spacing with about 3 mT was detected in this g = 5 (4.9) signal. The shift to g = 5 (4.9) was related to the distortion of the manganese cluster, derived to the modification of the chemical bond or the crystalline field of the Mn4(III) in the manganese cluster. Based on the EPR analysis of the g = 5 (4.9) spin state, another molecular structure of the S_2 state, a 'distant Mn' structure, was discussed as an intermediate state between the S_2 and S_3 states.

1.Introduction

Photosynthetic oxygen evolution is an indispensable reaction for life on earth. The Mn_4CaO_5 cluster, located in the photosystem II (PS II) protein complex, is the core machinery for oxygen evolution[1-3]. The Mn cluster has five different redox states denoted S_n (n = 0 – 4), where S_n advances to an S_{n+1} state by oxidation. S_4 is the highest oxidation state of the cluster, and it immediately relaxes to the lowest state S_0, with the evolution of molecular oxygen[4]. X-ray crystallographic techniques have revealed the high resolution structure of PS II[5-7]. The structure of the manganese cluster is called a 'distorted chair', which consists of the cube of Mn_3CaO_4 and additional Mn and oxygen. The Mn and O atoms in the cubic structure are labelled as Mn1-3 and O1-3,5, and the dangling Mn and bridging O are labelled as Mn4 and O4, respectively. The dangling Mn4 binds two water molecules, labelled W1 and W2, the surrounding amino acids and two O atoms in the Mn_4CaO_5 frame (Fig. 1) [5].

X-ray free electron laser (XFEL) studies showed that the distance between Mn1 and Mn4 is elongated and two oxygen atoms bridge the Mn1 and Mn4 in the S_3 state, which indicates that one oxygen atom is inserted in the transition of the S_2 to S_3 state. This structural change provides important clues for revealing the chemical mechanism of the evolution of an oxygen molecule [6, 7].

In the S_2 state, two kinds of EPR signals are mainly observed, called as the g = 2 multiline and g = 4.1 signals [8, 9]. The two signals are in equilibrium at temperatures above 200 K. The g = 4.1 signal has been characterized as the transition of the ±3/2 state at an effective spin $\boldsymbol{S}$ = 5/2 [10, 11]. Under physiological conditions, the g = 4.1 signal was not observed in cyanobacterial PS II. Besides, the g = 6-10 signals are found under specific conditions in the S_2 state [12, 13]; they are induced by infrared light below 65 K, and converted to the g = 2 multiline signal by annealing above 65 K in the spinach PS II [13].

Quantum chemical calculations have proposed two stable S_2 structures, open cubane (R-form) and closed cubane (L-form) forms [14, 15]. These structures are characterized by the position of the O5 oxygen between Mn1 and Mn4 [14, 15], in which the shorter Mn4-O5 and Mn1-O5 distances correspond to the open (R) and closed (L) cubane forms, respectively. Using density functional theory (DFT) calculations, Pantazis et al. have also linked the structures with the S_2 spin isomers, where the g = 2 multiline and g = 4.1 signals were assigned to the open and closed cubane structures, respectively [15]. However, quantum chemical calculations has not been successful in reproducing the closed cubane structure for g = 4.1 EPR signal in four-spin simulation [15]. The broad signals around g =6-10 thus was assigned to the closed cubane structure denoted as the '$g \geq 4$ signal' [15] . However, as the g = 4.1 and g = 6-10 signals originate from quite different states, it is inadequate that both the signals have been categorized as "$g \geq 4$ signals". Meanwhile, there is also some variety in the g = 4.1 signals in the range of g = 4-5 [16-19]. This variety of g = 4-5 is not in a negligible scale. In plant PS II, the *g*-factor of the signals has also been characterized as "$g \geq 4$ signals". On the relaxation process of the S_3 to S_2 states at cryogenic temperature, the signal with $g \sim 5$, denoted as S_2' state, was observed [16, 17]. This signal was converted to g = 4.1 after annealing to 220 K. The $g \sim 5$ signal thus has been proposed to be an intermediate between the S_2 and S_3 states. In cyanobacteria, the g = 4 signal is generally not detected under physiological conditions [18, 19]. However, Boussac et al. have reported the g = 4.7-4.9 signal at high pH in *Thermosynechococcus elongatus*, supporting that this state is an intermediate of the S_2-S_3 transition relevant to the g = 5 signal in spinach PS II

[18, 19]. The structural difference between g = 4 and 5 is an important clue to understand the S state transitions.

In this study, we focused on the effect of the extrinsic proteins, PsbO, PsbP and PsbQ, on the S_2 EPR signals. These proteins are essential for the oxygen evolving activity. The main difference between plant and cyanobacterial PS II core complexes exists in the extrinsic proteins, i.e., PsbO, PsbP and PsbQ are found in plant PS II, whereas the latter two are replaced with PsbV and PsbU in cyanobacterial PS II[20]. These proteins also bring about the variety of the S_1 state signals [21, 22]. Upon removal of the extrinsic proteins, high-concentration Ca^{2+} is required to retain the oxygen evolution activity [23]. The extrinsic proteins also stabilize the Mn_4CaO_5 cluster and protect it from the attack of exogenous reductants [24, 25]. In this paper, we report the EPR analysis of the g ~5 EPR signal in extrinsic proteins-depleted PS II in the presence of high-concentration of Ca^{2+}. We discuss the molecular structures of the g = 4 and g = 5 signal states, based on recent results [26].

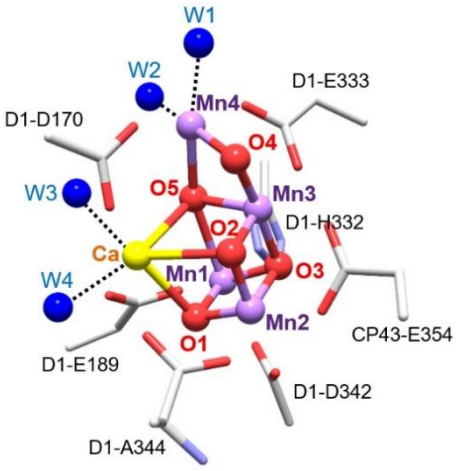

Figure 1 The model structure of the water oxidizing center of photosystem II (PDB:4ub6). The Mn_4CaO_5 cluster and its direct ligands, seven amino acid residues of D1 and CP43 subunits and four water molecules, are shown. Purple, yellow, and red spheres represent Mn, Ca, O atoms, respectively, while blue spheres represent water molecules.

2. MATERIALS AND METHODS

2.1. PS II sample preparation. PS II membranes were prepared from market spinach according to the method described previously[27]. The membranes were suspended in a buffer containing 400 mM sucrose, 5 mM NaCl, 5 mM $CaCl_2$, 0.5 mM EDTA•2Na and 40 mM Mes/NaOH (pH 6.0). The S_2 state was formed under white light illumination (500 W tungsten lamp) for 5 min at 200 K. All treatments were performed under dim green light at 4 ºC.

Depletion of the extrinsic proteins, PsbO/P/Q, was performed by 1 M $CaCl_2$ treatment [28], followed by resuspension in the above buffer. The membranes were also resuspended in buffers containing 100-1000 mM of $CaCl_2$, and 1000 mM of $SrCl_2$, NaCl and $MgCl_2$ for measurements with high-concentration cations.

2.2.EPR measurements. X-band CW-EPR measurements were carried out using a Bruker 300E EPR spectrometer with a super high Q resonator (ER 4122SHQ) and a gas flow temperature control system (ESR900, Oxford Instruments, Oxford, GB). All EPR measurements were performed at 6 K.

2.3.EPR calculations. EPR calculations were performed by MATLAB R2019a (The Mathworks, Inc) [26].

3.RESULTS

Figure 2 shows the EPR spectra of (a) untreated and (b-f) PsbO/P/Q-depleted PS II membranes in the presence of (b) 5, (c) 200, (d) 500, (e) 700, and (f) 1000 mM $CaCl_2$. The PSII membranes were illuminated at 200 K. The S_1 state spectra were subtracted from the S_2 state spectra (see Fig. S1). The signals at g ~ 4.3 and g ~ 3, which are ascribed to the rhombic iron and cytb559, respectively, were not completely subtracted.

Upon depletion of the extrinsic proteins, the g = 4 signal was largely reduced (trace b). However, the signal was recovered in the presence of high-concentration $CaCl_2$, and the effective g-factor was shifted toward ~5 (traces b-f).

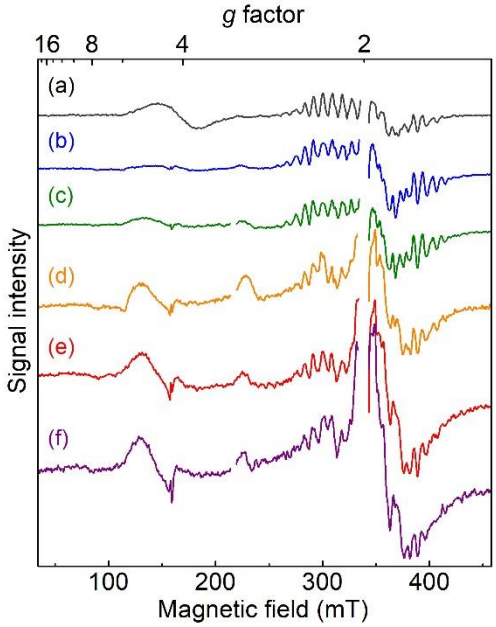

Figure 2. EPR spectra of the S_2 state in (a) the untreated PSII and (b-c) the PsbO/P/Q-depleted PS II in the presence of (b) 5, (c) 200, (d) 500, (e) 700, and (f) 1000 mM $CaCl_2$. The signal from $Y_D^{\bullet}$ (~340 mT) was removed. Gaps around 210 mT were also eliminated. Each spectrum was normalized by the average of the relatively clear peaks (2-4th left and 4-5th right from the center) of the g = 2 multiline signals. Experimental conditions: microwave frequency, 9.49 GHz; microwave power, 0.64 mW, modulation frequency, 100 kHz; modulation amplitude, 9 G.

Figure 3 shows the effect of cations in (a) the untreated PSII and (b-c) the PsbO/P/Q-depleted PS II in the presence of (b) 5 mM $CaCl_2$, (c) 1 M NaCl, (d) 1 M $MgCl_2$, (e) 1 M $CaCl_2$, and (f) 1 M $SrCl_2$. In the presence of 1 M divalent cations, Mg^{2+}, Ca^{2+}, and Sr^{2+}, the g = 4-5 signal was observed, whereas this

signal was not detected in the presence of the same concentration of a monovalent cation, Na^+. Figure 4 shows the relationship of the g = 4-5 signal intensities with the concentration of Ca^{2+} (b) and the metal species (c, Mg^{2+}; d, Sr^{2+}; e, Na^+) in the PsbO/P/Q-depleted PS II together with the intensity in the untreated PS II (a). The relative intensities of the g = 4-5 signal were initially evaluated by the peak-to-through, where the trough was taken as the left edge of the g = 4.3 spike signal when present, The signal was then normalized by the sum of the g = 4-5 and g = 2 multiline signals, and estimated under the assumption that the intensity ratio of the g = 4-5 signal and the g = 2 multiline is 0.5 in the untreated sample.

The mechanism of the Ca^{2+} concentration dependence is unclear. For simplification, we assumed a very weak binding site for the cation that is relevant for the spin conversion. The dotted line in Figure 4 was obtained by assuming that the equilibrium between the g = 4-5 state and the g = 2 multiline state depends on the concentration of Ca^{2+}. The equilibrium constant K_{Ca} (equation 1) was estimated to be > 300 mM.

$$K_{Ca} = \frac{[high\ spin\ state]}{[low\ spin\ state\ ][Ca^{2+}]} \qquad (1).$$

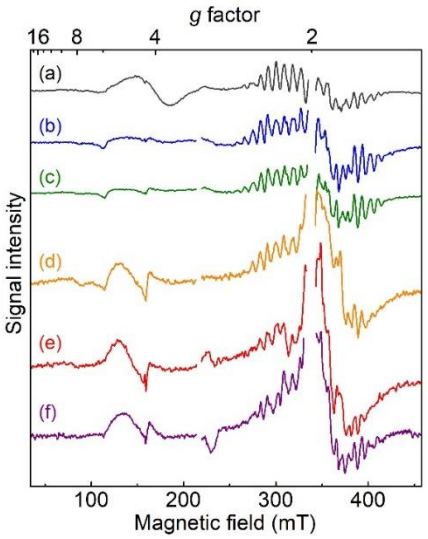

Figure 3. EPR spectra of the S_2 state in (a) the untreated PSII and (b-c) the PsbO/P/Q-depleted PS II in the presence of (b) 5 mM $CaCl_2$, (c) 1 M NaCl, (d) 1 M $MgCl_2$, (e) 1 M $CaCl_2$, and (f) 1 M $SrCl_2$. Each spectrum was normalized by the average of the relatively clear peaks (2-4th left and 4-5th right from the center) of the g = 2 multiline signals. Experimental conditions are the same as Fig. 2.

Figure 5 shows the expanded view of the g = 4-5 signals in (a) the untreated PSII, and the PsbO/P/Q-depleted PS II in the presence of (b) 200 mM and (c) 1 M $CaCl_2$. The spectra were obtained by subtraction of the S_1-state spectra from the S_2 spectra after annealing at 273 K. Short annealing of the S_2 state at 273 K for 2 s [19] enhanced the g = 4 signal by a factor of about 2 (Figure S1). In untreated PS II, the obtained g-factor was 4.1 (trace a). In the presence of 200 mM $CaCl_2$, the g = 4 signal was observed at g ~ 4.66, By further addition of $CaCl_2$ to 1 M, the signal was shifted to g ~ 4.9. The hyperfine structures, with 16-17 lines separated by about 3 mT, were observed in the spectrum centered at g = 4.86. Previously, Kim et al. reported the hyperfine structure of the g = 4.1 signal in the oriented NH_3-treated PS II, which was detected at the parallel direction to the membrane normal relative to the external field. Note that the hyperfine structure in the present work was detected in the powder spectrum, indicating that the effective g-anisotropy in the spin state is very small. The g = 4.9 signal would be identical to that in the previous reports, in which the signal was observed in spinach PS II in the relaxation process from the S_3 to S_2 states [16, 17] or in *T. elongatus* at high pH [18, 19].

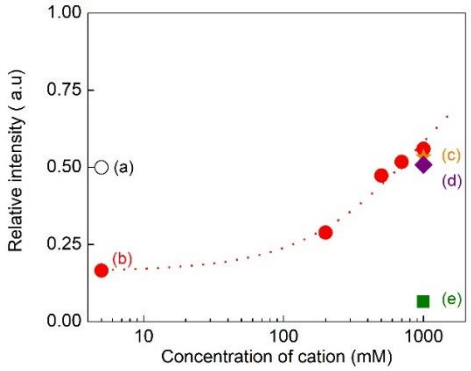

Figure 4. Relationship of the relative intensity of the g = 4-5 EPR signal with Ca^{2+} concentrations and metal species. (a, black open circle) untreated PSII; (b-e) PsbO/P/Q-depleted PS II in the presence of (b, red circles) 5-1000 mM $CaCl_2$, (c, orange diamond) 1 M $MgCl_2$, (d, purple diamond) 1 M $SrCl_2$, and (e, green square) 1 M NaCl. A dotted line represents the fitting curve of the Ca^{2+} concentration dependence in (b) with K_{Ca} = 1 M.

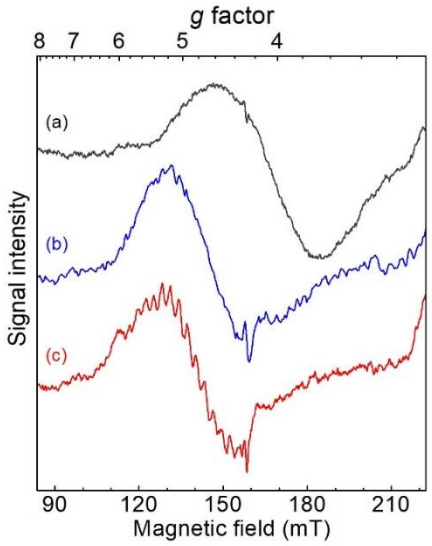

Figure 5. The g = 4-5 EPR signals of the S_2 state in (a) the untreated PS II (g = 4.1), and (b, c) the PsbO/P/Q-depleted PS

II in the presence of (b) 200 and (c) 1000 mM $CaCl_2$. The S_1-state spectra were subtracted from the S_2-state spectra after annealing at 273 K. Experimental conditions are the same as Fig. 2.

4.DISCUSSION

4.1. The g = 5 signal. The S_2 state has mainly two kinds of EPR signals, the g = 2 multiline signal and the g = 4 signal. The g = 2 multiline signal arises from the ground state of the $\boldsymbol{S}$ = 1/2 low spin state, while the g = 4 signal arises from the transition of the middle state $S = \pm 3/2$ in the $\boldsymbol{S}$ = 5/2 high spin state [9-11]. Quantum chemical calculations have suggested that S_2 state has two isomer structures, i.e., the open cubane (R-form) and closed cubane (L-form) forms [14, 15]. The low and high spin states were assigned to the open and closed cubane structures, respectively. The g = 4.1 signal was detected only in plant PS II under physiological conditions. We showed that the g = 5 signal shifts from the g = 4 signal in the PsbO/P/Q-depleted PS II in the presence of high-concentration divalent cations. The g-factor shift has been previously reported in the untreated spinach PSII [16, 17], where the signal at g = 5 appeared during the decay of the S_3 state at a cryogenic temperature, and subsequently the g = 5 signal converted to the normal g = 4.1 signal. Therefore, the g = 5 signal was assigned to the intermediate between the S_2 and S_3 states. The intermediate state was supported in the observation of the $g \sim 5$ signal in the process of the S_2 to S_3 transition in *T. elongatus* [18, 19]. In cyanobacterial PS II, this signal was detected only under high-pH conditions. The g-factor in *T. elongatus* PSII was estimated to be g = 4.75 [18, 19], which was slightly different from that in plant PS II. The g-factors under different conditions are summarized in Table 1. The g-factor was upshifted in the presence of high-concentration divalent cations in the PsbO/P/Q-depleted PS II, indicating that this shift is caused by a charge effect. In the presence of the extrinsic proteins, the Mn_4CaO_5 cluster may be less affected by the surface charge. In the absence of the extrinsic proteins, however, it is readily affected, which would cause the structural distortion of the Mn_4CaO_5 cluster. If both spinach and *T. elongatus* PS II complexes are regulated by the similar charge effect, the pH dependence of the g-factor observed in *T. elongatus* would be caused not by direct deprotonation of the Mn_4CaO_5 cluster but by the deprotonation of nearby amino acid residues, such as D1-His337.

4.2. Appearance of the hyperfine splittings in the g = 5 signal. In the presence of high-concentration Ca^{2+} in the PsbO/P/Q-depleted PS II, the g = 4-5 signal showed not only the g-factor shift but also resolving hyperfine splitting spacing with about 3 mT separations. In a single spin model, the spin Hamiltonian is described as[26]

$$\mathcal{H} = g\beta \boldsymbol{S}\boldsymbol{B_0} + D\left[\boldsymbol{S_z^2} - \frac{1}{3}S(S+1)\right] + E\left(\boldsymbol{S_x^2} - \boldsymbol{S_y^2}\right) + \sum \boldsymbol{I}\cdot\boldsymbol{A}\cdot\boldsymbol{S} \quad (2)$$

, where $\boldsymbol{S}$ and $\boldsymbol{I}$ are electron spin and nuclear spin operators, respectively, D and E are zero-field splitting (ZFS) parameters, g is a g-factor, $\boldsymbol{A}$ is a hyperfine tensor, and $\boldsymbol{S}$ is an effective spin operator. The effective g-factor is determined by the first three terms in eq (2). The anisotropy of the g = 4.1 signal is mainly ascribed to the zero-field splitting parameters, D and E, which have been well characterized by the rhombic parameter E/D = 0.25 [10, 11] . The x, y and z axes are approximately along the Mn4-W2, Mn4-E333 and Mn4-W1 axes, respectively [26]. The effective g-factors in the X-band were 4.0, 3.7, 4.7 for g_x, g_y, and g_z, respectively.

A d-electron system in the symmetrical crystalline field is close to g = 2, generally called the 'missing angular momentum' The g-factor of Mn(III) in the g = 4.1 signal has been assumed to be g = 2, which has been well reproduced in the experimental and calculated results [11, 15, 26]. The g-factor shift from 2 is derived from spin-orbital coupling caused by the distortion of the crystal field. Mn(III) in the octahedral symmetric field has four d electrons, occupying the dxy, dxz, dyz, and dx^2-y^2 (or dz^2) orbitals (Figure S2). This arrangement in the d4-electron system does not affect the spin-orbital interaction as the first approximation. An elongated/shortened bond in z direction is also insensitive to the g-factor under the conditions of degenerating dxy, dxz, dyz orbitals. These insights have been well supported by the simulation results [11, 26]. Therefore, the effective g = 4.1 indicates that Mn4 is in the axial symmetric crystalline field. The anisotropy in the Mn_4CaO_5 cluster is mainly explained by the onsite rhombic parameter, e/d, of the Mn(III) located in Mn4[26].

There are two possibilities for missing g-anisotropy of the g = 5 signals: (1) the spin system has $\boldsymbol{S}$ = 7/2 with g = 2, and the crystalline field is a axial symmetry, i.e., E/D (e/d) ~0.11; (2) the spin system has $\boldsymbol{S}$ = 5/2, and the crystalline field is a rhombic symmetry, i.e., E/D (e/d) ~0.33. Figure 6 shows the rhombic parameter dependence of the effective g-factor of the g = 4.9 signal. In the case of the $\boldsymbol{S}$ = 7/2 system, E/D ~0.11 gives a good solution, in agreement with the previous report, in which the g = 5 signal was assigned to $\boldsymbol{S}$ = 7/2 with g = 2 [16]. In the case of the $\boldsymbol{S}$ = 5/2 spin system, the rhombic symmetry E/D = 0.33 gives g = 2.32. Table S1 shows the possible g-anisotropy at a different E/D ratio.

Table 1: Experimental parameters of the g = 4-5 signals in PS II

	Effective g-factor	Linewidth (mT)	Hyperfine separation (mT)
spinach [*1] (untreated)	4.09	38.9	n.d.
spinach [*1] (with 1 M $CaCl_2$)	4.86	22.8	3.1
spinach [*2] (S_3 relaxation at 77 K)	4.7	27	n.d.
T. elongatus [*3] (at high pH)	4.75	24	n.d.
spinach [*4] (in oriented, NH_3-treated)	4.1	26	3.6

[*1] this work, [*2] estimated from refs. [16, 17], [*3] estimated from refs. [18, 19], [*4] estimated from ref.[29] . The linewidth was evaluated as a peak-to-peak separation.

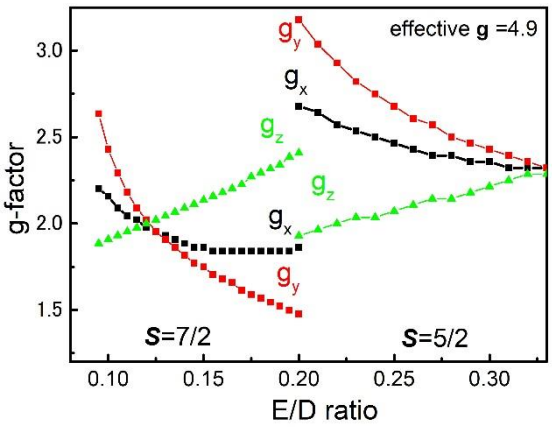

Figure 6. Conditions for the isotropic g_{eff} = 4.9 signal. The *g*-factor for each *xyz* axis in the $\boldsymbol{S}$ = 5/2 or $\boldsymbol{S}$ = 7/2 spin system with $D = -0.455$ cm^{-1}.

The *g* = 5 signal is observable only in a limited magnetic structure. Nevertheless, the *g* = 5 signals are detected in various conditions, e.g., during S_3 relaxation at a cryogenic temperature in untreated spinach [16, 17], at high pH in *T. elongatus* [18, 19], and in the presence of high-concentration Ca^{2+} in extrinsic protein-depleted PSII, indicating that these signals originate from a similar S_2 structure, albeit slightly different *g*-factors depending on the environmental conditions.

Figure 7 shows (a) the experimental and (b, c) simulated spectra of the *g* = 5 (4.9) signal. The experimental spectrum was obtained by subtraction of the spectrum before annealing at 273 K from that after annealing in the S_2 state. The subtraction better eliminates an unwanted spike signal observed at *g* = 4.3. The *g*-factor of *g*=4.86±0.10 was estimated from the symmetry of the spectrum with the hyperfine structure. The error range on the subtraction procedure was evaluated as the spacing of the next hyperfine lines.

The simulation was evaluated using the spacing of the central part of the spectrum and the whole linewidth. The effective isotropic *g* = 4.9 was used for simulation. A set of four isotropic hyperfine splittings, A_1 = 1.4 mT, A_2 = 1.5 mT, A_3 = 1.5 mT, and A_4 = 2.6 mT, were used. Kim et al. have used the hyperfine set of four isotropic hyperfine constants, 4.5, 3.7, 3.4, and 1.6 mT, for the *g* = 4.1 signal in the oriented NH_3-treated PS II observed at 0°[29]. The present parameters are slightly smaller than those for the NH_3-treated PS II. This is consistent with the narrowing of the whole spectral line width, which is caused by the hyperfine narrowing with an increase of the *g*-factor (Table 1).

The hyperfine structure readily disappears by introducing small *g*-anisotropy. Fig. 7(c) shows the trial simulation including *g*-anisotropy. The hyperfine structure disappeared by the anisotropy of $\Delta g \sim 0.3$, which would rationally explain the shift of the effective *g*-factor in the intermediates with *g* = 4-5 in spinach PS II and in *T. elongatus* PSII at high pH.

4.3. Modified Structure of the S_2 state

We have recently reported that the anisotropy of the *g* = 4.1 signal is ascribed to Mn4(III) [26]. If the *g* = 5 signal arises from the $\boldsymbol{S}$ = 7/2 spin system, the crystalline field surrounding Mn(III) is close to the axial symmetry (Fig.6), but some structural change should take place in the conversion from the $\boldsymbol{S}$ = 5/2 *g* = 4 state to the $\boldsymbol{S}$ = 7/2 *g* = 5 state. The most plausible structure for the $\boldsymbol{S}$ = 7/2 state is a monomer/trimer structure, as shown in an early report[30]. The structure of the manganese cluster consists of the Mn_3CaO_4 cube and an additional Mn(Mn4) atom with an oxo bridge (O4). The change in the spin topology may be ascribed to the breakage between Mn4 and the cube, resulting in the monomer/trimer structure. Using a two spin coupling model for simplification, the $\boldsymbol{S}$ = 7/2 spin state is described as ferro-coupling between $\boldsymbol{S}$ = 2 (Mn4) and $\boldsymbol{S}$ = 3/2 (cube). This contrasts to the *g* = 4 spin system, where the $\boldsymbol{S}$ = 5/2 spin state is described as antiferro-coupling between $\boldsymbol{S}$ = 2 (Mn4) and $\boldsymbol{S}$ = 9/2 (cube).

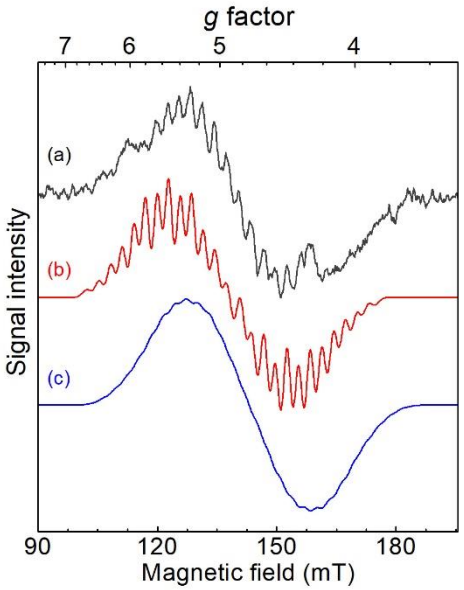

Figure 7. (a) Experimental and (b, c) simulated EPR spectra of the g = 4-5 signal. The experimental spectrum was obtained by subtraction of the spectrum before annealing at 273 K after 200 K illumination from that after annealing. The simulation parameters: four hyperfine coupling constants A_1 = 14 G, A_2 = 15 G, A_3 = 15 G, and A_4 = 26 G; effective *g*-factors, (b) 4.9 for $g_{eff,xyz}$, and (c) 4.75, 4.6, and 4.9 for $g_{eff,x}$, $g_{eff,y}$, and $g_{eff,z}$, respectively.

In the case of the $\boldsymbol{S}$ = 5/2 spin system for the *g* = 5 signal, the crystalline field surrounding Mn(III) should have an approximately orthorhombic symmetry (Figure S2A). As distortion on the *xy* plane (*E/D*) does not contribute to the *g*-factor shift largely in itself, leaning of the *z* direction should be involved. We have determined the *z* direction to be Mn-W1 for the *g* = 4.1 signal [26]. Thus, the crystalline field should be forced to lean

toward the O5-Mn4-W1 bond axis. Therefore, the movement of the *z* axis, including Mn4-W1 or Mn4-O5, may be essential for the *g*-factor shift. Recent quantum chemical calculations have shown the possibility of the distortion of the Mn4 crystalline field in the S_2 state [31].

Recent XFEL results showed the elongation of the distance between Mn1 and Mn4 and insertion of two oxygen atoms in the S_3 state, i.e., distant Mn1-Mn4 structure [6, 7]. According to this model, one oxygen is inserted between Mn1 and Mn4 upon extraction of an electron. The electron transfer event also incorporates the modification of the surrounding protein coordinates. In untreated spinach PSII, the g = 5 signal state was suggested to be an intermediate during the relaxation of the S_3 to the S_2 states at a cryogenic temperature [16, 17]. If the long distance between Mn1 and Mn4 or the modification of the z axis of Mn4 remains in the intermediate upon electron donation from Y_Z, this S_2 intermediate may give the g = 5 signal, where the monomer/trimer coupling appears in the cluster ($\boldsymbol{S}$ =7/2) or the crystalline field of Mn4 is distorted ($\boldsymbol{S}$=5/2). In the forward process of the S_2 to S_3 transition, the intermediate g = 5 structure would be transiently formed. The g = 5 intermediate state should have a slightly higher energy than the g = 2 and g = 4.1 states in the untreated PSII. In contrast, the g = 5 state in the extrinsic protein-depleted PS II with a high-concentration divalent cation or in *T. elongatus* PS II at high pH may be relatively stabilized by the charge effect of the surroundings of the manganese cluster. The model is summarized in Fig. 8. The observations are as follows: (1)The Mn1-Mn4 distance is larger in the S_3 state due to the insertion of an additional oxygen atom [6, 7]; (2) The g = 5 state shows the distortion of the Mn4 coordinates in the S_2 state (this work); (3) The g = 5 signal state is an intermediate state between the S_2 (the g = 4 state) and S_3 states [16-19]. These observations show that the insertion of an O-O bond is triggered from the g = 5 structure. On the other hand, the g = 5 signal is detected in the relaxation from the S_3 to S_2 states at 77 K[16]. Therefore, a weakly bound oxygen might be still located in the vicinity of Mn4 on the relaxation process at 77 K. The intermediate g = 5 state is proposed to have a 'distant Mn' structure with a Mn1-Mn4 distance similar to that in the S_3 state or with a distorted crystalline field of Mn4.

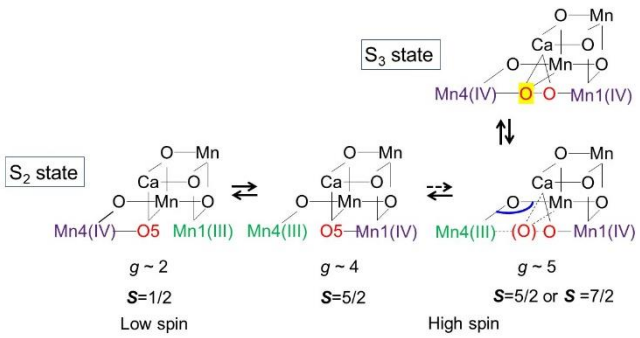

Figure 8. The structural model of the S_2 and S_3 states based on the present EPR study and the previous XFEL results [6, 7]. The Mn1-Mn4 distance is larger in the S_3 state due to the insertion of an additional oxygen atom [6, 7].

4.4. Comparison of the g = 5 signal state with the closed structure (g = 4.1) based on quantum chemical calculations

Quantum chemical calculations have proposed two isomers in the S_2 state with the open and closed cubane structures with Mn(III) at Mn1 and Mn4, respectively [14, 15]. The low spin state ($\boldsymbol{S}$ = 1/2) with the g ~ 2 multiline EPR signal was assigned to the open cubane (R) structure, whereas the high spin state ($\boldsymbol{S}$ = 5/2) with the g ~ 4 EPR signal was assigned to the closed cubane (L) structure. It was experimentally supported that Mn4 is Mn(III) in the g = 4 spin state [26]. However, the closed cubane model obtained by the quantum chemical calculation does not provide the g = 4.1 signal, because the mixing of the ground state and the weakly excited level derives the downshift of the g-factor[26].

In contrast, the possibility cannot be excluded that the closed cubane model by the quantum chemical calculation [14, 15] is similar to the structure of the g = 5 signal state. In this case, the calculation should be reevaluated as the ground state $\boldsymbol{S}$ = 7/2 or $\boldsymbol{S}$ = 5/2 with a shifted *g*-factor in an asymmetrical crystalline field. The quantum chemical calculations using spin-orbital couplings for the *g*-factor shift have not yet been performed. Although it might be challenging subject in this field, the spin-orbital interaction should be included in calculation for accurate estimation of the S_2 state structures.

5. CONCLUSIONS

The shift of the g = 4.1 signal was detected in the PsbO/P/Q-depleted PS II. The effective *g*-factor of the signal shifts up to ~5(4.9), depending on the divalent cation concentration. In addition to the shift of the effective *g*-factor, the hyperfine structure spacing with about 3 mT was detected. The shift was related to the breakage of the chemical coupling or the distortion of the crystalline field of the Mn4(III) in the S_2 state manganese cluster. Regarding the g = 5 signals as the intermediate states between the S_2 and S_3 states, another S_2 structure with a 'distant Mn' was proposed.

ASSOCIATED CONTENT

Supporting Information. **Figure S1**: EPR spectra of PsbO/P/Q-depleted PS II membranes of spinach in the presence of 1 M $CaCl_2$; **Figure S2**, the relationship between d electrons in the crystalline field and the g-factor; **Table S1**, the calculated anisotropic parameters for the g = 4.1 and 4.9 signals.

AUTHOR INFORMATION

Corresponding Author

*** mino@bio.phys.nagoya-u.ac.jp**

Author Contributions

The manuscript was written through contributions of all authors. / All authors have given approval to the final version of the manuscript.

ACKNOWLEDGMENT

This work was partly supported by a Nanotechnology Platform Program (Molecule and Material Synthesis) of the Ministry of Education, Culture, Sports, Science and Technology (MEXT), Japan (to H.M), and by JSPS KAKENHI Grant Number JP20H05096 (to H.M.) JP17H06435, JP17H03662, JP17H06433 (to T.N.).

ABBREVIATIONS

EPR, electron paramagnetic resonance; PS II, photosystem II.

REFERENCES

(1) McEvoy, J. P.; Brudvig, G. W. Water-splitting chemistry of photosystem II. *Chem. Rev.* **2006,** *106*, 4455-4483.
(2) Renger, G. *Functional Pattern of Photosystem II*. 2007; Vol. 9, p 237-290.
(3) Lubitz, W.; Chrysina, M.; Cox, N. Water oxidation in photosystem II. *Photosynth. Res.* **2019**.
(4) Kok, B.; Forbush, B.; McGloin, M. Cooperation of Charges in Photosynthetic O_2 Evolution.1. A Linear 4 Step Mechanism. *Photochem. Photobiol.* **1970,** *11*, 457-475.
(5) Umena, Y.; Kawakami, K.; Shen, J. R.; Kamiya, N. Crystal structure of oxygen-evolving photosystem II at a resolution of 1.9 Å. *Nature* **2011,** *473*, 55-60.
(6) Kern, J.; Chatterjee, R.; Young, I. D.; Fuller, F. D.; Lassalle, L.; Ibrahim, M.; Gul, S.; Fransson, T.; Brewster, A. S.; Alonso-Mori, R.*, et al.* Structures of the intermediates of Kok's photosynthetic water oxidation clock. *Nature* **2018,** *563*, 421-425.
(7) Suga, M.; Akita, F.; Yamashita, K.; Nakajima, Y.; Ueno, G.; Li, H.; Yamane, T.; Hirata, K.; Umena, Y.; Yonekura, S.*, et al.* An oxyl/oxo mechanism for oxygen-oxygen coupling in PSII revealed by an x-ray free-electron laser. *Science* **2019,** *366*, 334-338.
(8) Casey, J. L.; Sauer, K. Electron-Paramagnetic-Res Detection of a Cryogenically Photogenerated Intermediate in Photosynthetic Oxygen Evolution. *Biochim. Biophys. Acta* **1984,** *767*, 21-28.
(9) de Paula, J. C.; Beck, W. F.; Miller, A. F.; Wilson, R. B.; Brudvig, G. W. Studies of the Manganese Site of Photosystem II by Electron Spin Resonance Spectroscopy. *J. Chem. Soc., Faraday Trans. 1* **1987,** *83*, 3635-3651.
(10) Astashkin, A. V.; Kodera, Y.; Kawamori, A. Pulsed EPR Study of Manganese *g*=4.1 Signal in Plant Photosystem II. *J. Magn. Reson. B.* **1994,** *105*, 113-119.
(11) Haddy, A.; Lakshmi, K. V.; Brudvig, G. W.; Frank, H. A. Q-band EPR of the S_2 state of Photosystem II confirms an S=5/2 origin of the X-band *g*=4.1 signal. *Biophys. J.* **2004,** *87*, 2885-2896.
(12) Boussac, A.; Kuhl, H.; Un, S.; Rogner, M.; Rutherford, A. W. Effect of near-infrared light on the S-2-state of the manganese complex of photosystem II from Synechococcus elongatus. *Biochemistry* **1998,** *37*, 8995-9000.
(13) Boussac, A.; Un, S.; Horner, O.; Rutherford, A. W. High-spin states (S >= 5/2) of the photosystem II manganese complex. *Biochemistry* **1998,** *37*, 4001-4007.
(14) Isobe, H.; Shoji, M.; Yamanaka, S.; Umena, Y.; Kawakami, K.; Kamiya, N.; Shen, J. R.; Yamaguchi, K. Theoretical Illumination of Water-inserted Structures of the $CaMn_4O_5$ cluster in the S_2 and S_3 States of Oxygen-Evolving Complex of photosystem II: Full Geometry Optimizations by B3LYP Hybrid Density Functional. *Dalton Trans.* **2012,** *41*, 13727-13740.
(15) Pantazis, D. A.; Ames, W.; Cox, N.; Lubitz, W.; Neese, F. Two interconvertible structures that explain the spectroscopic properties of the oxygen-evolving complex of photosystem II in the S_2 state. *Angew. Chem. Int. Ed. Engl.* **2012,** *51*, 9935-9940.
(16) Ioannidis, N.; Petrouleas, V. Decay products of the S_3 state of the oxygen-evolving complex of photosystem II at cryogenic temperatures. Pathways to the formation of the S=7/2 S_2 state configuration. *Biochemistry* **2002,** *41*, 9580-9588.
(17) Ioannidis, N.; Nugent, J. H. A.; Petrouleas, V. Intermediates of the S_3 state of the oxygen-evolving complex of photosystem II. *Biochemistry* **2002,** *41*, 9589-9600.
(18) Boussac, A. Temperature dependence of the high-spin S_2 to S_3 transition in Photosystem II: Mechanistic consequences. *Biochim. Biophys. Acta* **2019,** *1860*, 508-518.
(19) Boussac, A.; Ugur, I.; Marion, A.; Sugiura, M.; Kaila, V. R. I.; Rutherford, A. W. The low spin - high spin equilibrium in the S_2-state of the water oxidizing enzyme. *Biochim. Biophys. Acta* **2018,** *1859*, 342-356.
(20) Ifuku, K.; Noguchi, T. Structural Coupling of Extrinsic Proteins with the Oxygen-Evolving Center in Photosystem II. *Front. Plant Sci.* **2016,** *7*, 84.
(21) Matsukawa, T.; Mino, H.; Yoneda, D.; Kawamori, A. Dual-mode EPR study of new signals from the S_3-state of oxygen-evolving complex in photosystem II. *Biochemistry* **1999,** *38*, 4072-4077.
(22) Campbell, K. A.; Peloquin, J. M.; Pham, D. P.; Debus, R. J.; Britt, R. D. Parallel polarization EPR detection of an S_1-state "multiline" EPR signal in photosystem II particles from Synechocystis sp. PCC 6803. *J. Am. Chem. Soc.* **1998,** *120*, 447-448.
(23) Ghanotakis, D. F.; Topper, J. N.; Babcock, G. T.; Yocum, C. F. Water-soluble 17 kDa and 23 kDa polypeptides restore oxygen evolution activity by creating a high-affinity binding saite for Ca^{2+} on the oxidizing side of Photosystem II. *FEBS Lett.* **1984,** *170*, 169-173.
(24) Ghanotakis, D. F.; Topper, J. N.; Yocum, C. F. Structural organization of the oxidizing side of Photosystem II - exogenous reductants reduce and destroy the Mn-complex in shotosystems II membranes depleted of the 17 and 23 kDa. *Biochim. Biophys. Acta* **1984,** *767*, 524-531.
(25) Kuwabara, T.; Miyao, M.; Murata, T.; Murata, N. The function of 33-kDa protein in the photosynthetic oxygen-evolution system studied by reconstitution experiments. *Biochim. Biophys. Acta* **1985,** *806*, 283-289.
(26) Mino, H.; Nagashima, H. Orientation of Ligand Field for Dangling Manganese in Photosynthetic Oxygen-Evolving Complex of Photosystem II. *J. Phys. Chem. B* **2020,** *124*, 128-133.
(27) Nagashima, H.; Mino, H. Highly resolved proton matrix ENDOR of oriented photosystem II membranes in the S_2 state. *Biochim. Biophys. Acta* **2013,** *1827*, 1165-1173.
(28) Tomita, M.; Ifuku, K.; Sato, F.; Noguchi, T. FTIR Evidence That the PsbP Extrinsic Protein Induces Protein Conformational Changes around the Oxygen-Evolving Mn Cluster in Photosystem II. *Biochemistry* **2009,** *48*, 6318-6325.
(29) Kim, D. H.; Britt, R. D.; Klein, M. P.; Sauer, K. The Manganese Site of the Photosynthetic Oxygen-Evolving Complex Probed by EPR Spectroscopy of Oriented Photosystem II Membranes: the g = 4 and g = 2 Multiline Signals. *Biochemistry* **1992,** *31*, 541-547.

(30) Peloquin, J. M.; Campbell, K. A.; Randall, D. W.; Evanchik, M. A.; Pecoraro, V. L.; Armstrong, W. H.; Britt, R. D. ^{55}Mn ENDOR of the S_2 state multiline EPR signal of photosystem II: Implications on the structure of the tetranuclear Mn cluster. *J. Am. Chem. Soc.* **2000,** *122*, 10926-10942.
(31) Miyagawa, K.; Isobe, H.; Kawakami, T.; Shoji, M.; Yamanaka, S.; Okumura, M.; Nakajima, T.; Yamaguchi, K. Domain-based local pair natural orbital CCSD(T) calculations of fourteen different S_2 intermediates for water oxidation in the Kok cycle of OEC of PS II. Re-visit to one LS-two HS model for the S_2 state. *Chem. Phys. Lett.* **2019**, 136731.

TOC Graphic

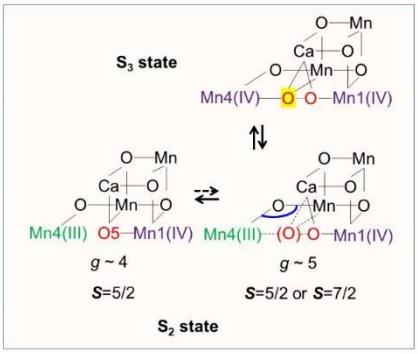
S3 state
O—Mn
Ca—O
O—Mn—O
Mn4(IV)—O—O—Mn1(IV)
O—Mn
Ca—O
O—Mn—O
Mn4(III) O5—Mn1(IV)
g ~ 4
S=5/2
O—Mn
Ca—O
O—Mn—O
Mn4(III)···(O)—O—Mn1(IV)
g ~ 5
S=5/2 or S=7/2
S2 state